

# Three-Dimensional Relativistic Jet Simulations of Radio-Loud Active Galactic Nuclei (AGN)

Terance Schuh,<sup>1, a)</sup> Yutong Li,<sup>2</sup> and Paul J. Wiita<sup>1</sup>

<sup>1</sup>*Department of Physics, The College of New Jersey, Ewing, New Jersey 08618, USA*

<sup>2</sup>*Institute of Space Sciences, Shandong University, Weihai, People's Republic of China*

Corresponding Author <sup>a)</sup>schuht1@tcnj.edu

**Abstract.** We have computed a suite of simulations of propagating three-dimensional relativistic jets involving substantial ranges of initial jet Lorentz factors and ratios of jet density to external medium density. These allow us to categorize the respective active galactic nuclei (AGN) into Fanaroff–Riley (FR) class I (jet dominated) and FR class II (lobe dominated) based upon the stability and morphology of the simulations. We used the Athena code, and more recently, the Athena++ code, to produce a collection of large 3D variations of jets, many of which propagate stably and quickly for over 100 jet radii, but others of which eventually become unstable and fill up slowing advancing lobes. Comparing the times when some jets become unstable to these initial parameters allows us to find a threshold where radio-loud AGNs transition from class II to class I. With our highest resolution, fully 3D relativistic simulations we can represent the jets more accurately and thus improve upon and refine earlier results that were based on both our now high-resolution 3D and 2D simulations.

## INTRODUCTION

Active galactic nuclei (AGN) are galaxies that not only have a supermassive black hole at the center but also emit an intense amount of radiation solely due to the black hole and not the surrounding stars within the galaxy. The black hole is so large and in the process of consuming so much matter that it causes the material it has not yet swallowed to generate so much energy that compared to all the light produced from the billions of stars in the respective galaxy, we see only the radiation due to the black hole! A small percentage of these AGN, around 10%, are classified as radio loud,<sup>1</sup> primarily meaning that they are characterized by relativistic plasma jets extending from the north and/or south poles of the black hole. These jets are linear structures that transport energy and particles at speeds near the speed of light from the compact central region of the AGN out to thousands of parsecs or sometimes even millions of parsecs in length. Another important characteristic of these jet structures is that they emit synchrotron radiation, an observational phenomenon where charged particles such as electrons spiral around magnetic fields, again causing large amounts of radiation to be emitted across the electromagnetic spectrum.<sup>2</sup> Due to the uniqueness and high energy of these radio-loud AGN we desire to understand their underlying physics.

## FR I and FR II

The previously described radio jets have long been classified into two categories based upon their radio morphology.<sup>3</sup> Fanaroff-Riley I (FR I) sources have jet-dominated emission and are weaker, with the majority of their radiation arising from the inner halves. The FR II, on the other hand, or classical double sources, have emission dominated by lobes containing terminal hot spots. Furthermore, some hybrid-morphology radio sources (HYMORS) have been discovered that show FR I structure on one side of the radio source and FR II morphology on the other.<sup>4</sup> These sources are important in understanding the basic origin of the FR I and FR II dichotomy, where the different morphologies may be induced by intrinsically different jet properties, interactions with different environments on

either side of the source, or long-term temporal variations combined with the time lag in the observer’s frame between evolving approaching and receding lobes.

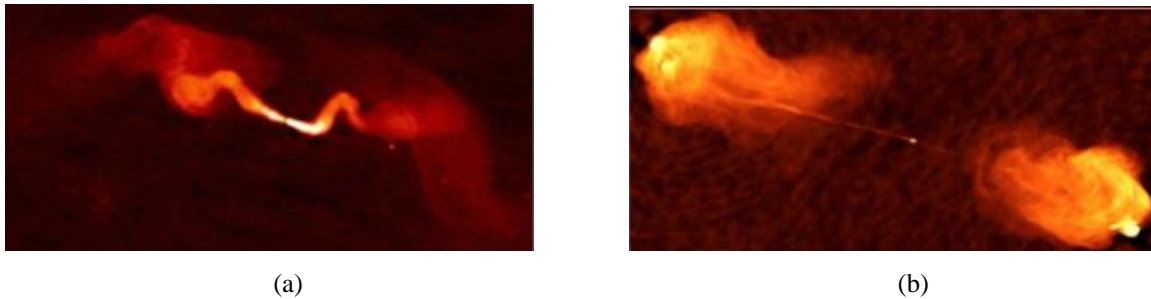


**FIGURE 1.** Two radio galaxies with jets seen using a radiograph. (a) An example of a FR I–type AGN, specifically, radio galaxy 3C 31. Image courtesy of the NRAO/AUI. (b) An example of a FR II–type AGN, specifically, Cygnus A. Image courtesy of the VLA.

## METHOD OF RESEARCH

FR I or FR II type, these radio-loud AGN are impossible to physically create here on Earth, so like most astrophysical research, to study the astronomical objects we computationally model them using supercomputers. Because the jets are comprised of plasma, we can effectively treat them as a fluid; thus we employ hydrodynamical computer codes to generate our models. These hydrodynamical simulations of propagating jets are of critical importance to the understanding of radio galaxies and now have a history spanning four decades.<sup>5–7</sup> These simulations give fundamental support to the idea of the twin-jet models for radio galaxies.<sup>8, 9</sup> Like most computational work, the complexity of the simulations has increased in parallel with growing computational power and algorithm development, leading to a better understanding of the jet phenomenon, focusing on the study of the morphology, dynamics, and nonlinear stability of jets at kiloparsec and larger scales.

To perform our specific research we used The College of New Jersey’s ELSA High Performance Computing Cluster in parallel with the Athena code and its successor Athena++, both developed by Stone and colleagues.<sup>10–13</sup> Both codes are highly efficient, grid-based codes for astrophysical magnetohydrodynamics (MHD) that were developed primarily for studies of the interstellar medium, star formation, and accretion flows. Athena++ has the capability to include special relativistic hydrodynamics (RHD), MHD, static (fixed) mesh refinement, and parallelization. The discretization is based on cell-centered volume averages for mass, momentum, and energy, and face-centered area averages for the magnetic field. In order to solve a series of partial differential equations expressing conservation laws, the rest density, pressure, velocity, internal energy, and magnetic field are calculated in the strictly RHD simulations with the magnetic field set to zero.

With the goal to understand the physics and characteristics of FR I– and FR II–type jets, we have simulated these propagating jets and created a very extensive suite of both medium- and high-power jets in three dimensions. Much previous work has been devoted to modeling relativistic jets in two dimensions rather than three dimensions due to a lack of computational power,<sup>14</sup> so after a thorough literature search, to our knowledge we are among the first research groups to model these large-scale jets three dimensionally while maintaining high resolution. Since in reality the jets are three dimensional, this enhancement allows us to classify them more accurately, making better predictions concerning the jets and developing a stronger understanding of them.

## SIMULATIONS

We use the Athena code for special relativistic hydrodynamics and the Athena++ code for special relativistic MHD. These codes allow us to produce 3D simulations of jets propagating through initially uniform external or ambient media with a wide range of power. To model our jets, the initial physical parameters of jet velocity  $v_j$  (assumed constant across the cross section for our initially cylindrical jets), proper ambient and jet densities ( $\rho_a$  and  $\rho_j$ , respectively), ambient and jet pressures ( $P_a$  and  $P_j$ ), magnetic fields ( $B_{jet}$  and  $B_{amb}$ ), and adiabatic index  $\Gamma$  must be specified. Of these, the dominant variables are  $v_j$  and  $\eta = \rho_j/\rho_a$ , and these are the ones we discuss. In the MHD simulations the magnetic fields are also dominant variables, but because we have not been able to produce fully high-resolution 3D relativistic MHD simulations, we will not discuss them here.

With substantial experimentation involving different code parameters, our best overall results for faster jets came from simulations of highest resolution (HHR) 3D RHD jets with  $1200 \times 1000 \times 1000$  zones with 20 zones per grid. Previously our highest resolution had been  $600 \times 500 \times 500$  zones with 10 zones per grid. We now classify this resolution as high resolution (HR). Most recently, upwards of 60 HR RHD simulations have now successfully been performed with the Athena code with different combinations of jet velocities ( $v_j$ ) and jet-to-ambient matter density ratios ( $\eta$ ). Of these HR simulations we have been able to reproduce more than 10 of them at our new higher resolution (HHR). The simulations contain a range of  $\eta$  from 0.0005 to 0.0316 and a range of initial  $v_j$  from  $0.7c$  to  $0.995c$ . A summary of the results of these simulations is shown in Fig. 2. The circles in the figure represent runs with jets that eventually become unstable before the end of the grid at 60 or 120 jet radii is reached. This characteristic is intrinsic of FR I radio sources and is the reason why these sources, when scaled to extragalactic dimensions, appear the way they do (see Fig. 1a). The instability is created because the core of the jet is not powerful enough to propagate past a certain threshold on the grid, either due to  $v_j$ ,  $\eta$ , or a combination of the two. On the contrary, triangles show parameters of runs with jets that are powerful enough to remain stable enough throughout the entire simulation (to even 240 jet radii) and thus are plausibly representative of FR II sources (see Fig. 1b).

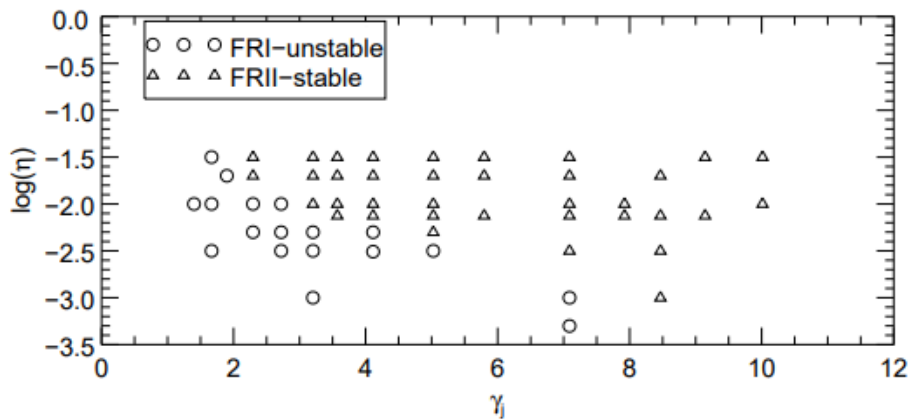


**FIGURE 2.** A summary of the stability of 54 jets. Note that these are our HR simulations. A subset of these have been produced using HHR. The x-axis is an alternate way of expressing  $v_j$  (a larger value corresponds to a faster jet), and the y-axis is a log scale of  $\eta = \frac{\rho_j}{\rho_a}$ . Circles represent FR I runs which have unstable jets; triangles are FR II runs with stable jets.

## RESULTS AND ANALYSIS

For simplicity, rather than analyzing data from several runs and determining the overall results, we examine one FR I jet simulation but at the two resolution types and draw conclusions using this approach. The jet we focus on had parameters  $v_j = 0.80c$  and  $\eta = 0.00316$ . The HR simulation had  $600 \times 400 \times 400$  zones with 10 zones per grid, and the HHR simulation had  $1200 \times 800 \times 800$  zones with 20 zones per grid.

The first step in analyzing any run is always identifying whether the jet becomes unstable, and if so, finding precisely when it does. In this specific case, we suspected our jet would be of the FR I variety, which it was, so thus we concerned ourselves with finding the point of instability. If we look at a short time lapse of the HR simulation, Fig. 3, we see everything begins stable at  $t = 0$  and remains so up until approximately  $t = 300$ . Not shown, the instability first occurs at around  $t = 330$ , but its effects are especially evident at  $t = 450$  because the jet (dark blue region) now appears wavy. It is clear it has lost its stability. As time goes on we continue to see the jet in its entirety propagate toward the edge of the grid, but the jet end (dark blue column region) has come to a stop at around 30 jet radii, while both the cocoon (dark blue balloonlike region) and bow shock (red region) continue to propagate, now more slowly, toward the edge of the grid. Having identified the location of instability (30 jet radii), we compare the simulation to its HHR counterpart. By doing so, we can draw conclusions about the differences between the resolution types.

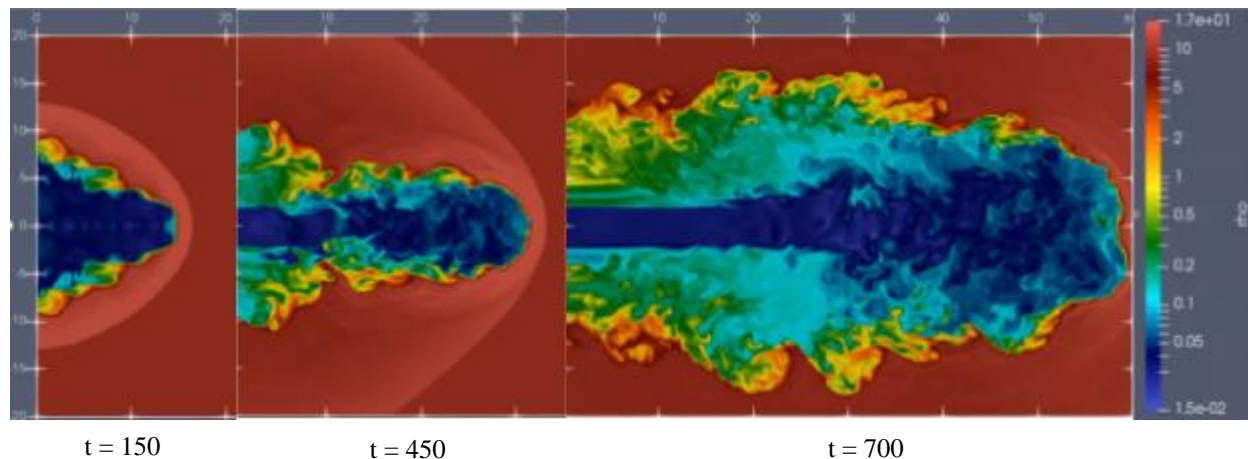


**FIGURE 3.** HR jet simulation with parameters  $v_j = 0.80c$  and  $\eta = 0.00316$ . This simulation is an FR I type. We see that by  $t = 450$ , the jet has become unstable. This is seen by the waviness of the dark blue region. As the simulation continues, the jet itself (dark blue column region) remains nearly fixed at 30 jet radii, while other features such as the cocoon (dark blue balloonlike region) and bow shock (red region) propagate further and reach the edge of the grid.

Now examining the HHR simulation, we again look for the point where the jet goes unstable. Remember the parameters of this jet are identical. Looking at a time lapse, Fig. 4, we see everything begins stable at  $t = 0$ , as expected. Like the HR simulation, the jet begins to become unstable at around  $t = 300$ . After 100–200 time steps, later it is clear the jet has indeed become unstable, as seen by the wavy feature of the dark blue region. As the jet continues propagating, everything seems identical, except for the fact that we are at a higher resolution. Taking a closer look, we see that our HHR simulation propagates for the same amount of time as the HR version, but it does not propagate as far. We also notice that the jet end (dark blue column region) of the HHR simulation is at approximately 25 jet radii, which is 5 jet radii less than before. At first this is surprising, but it is actually somewhat expected. Because we are at a higher resolution now, the code is performing many more calculations. This is going to make propagation

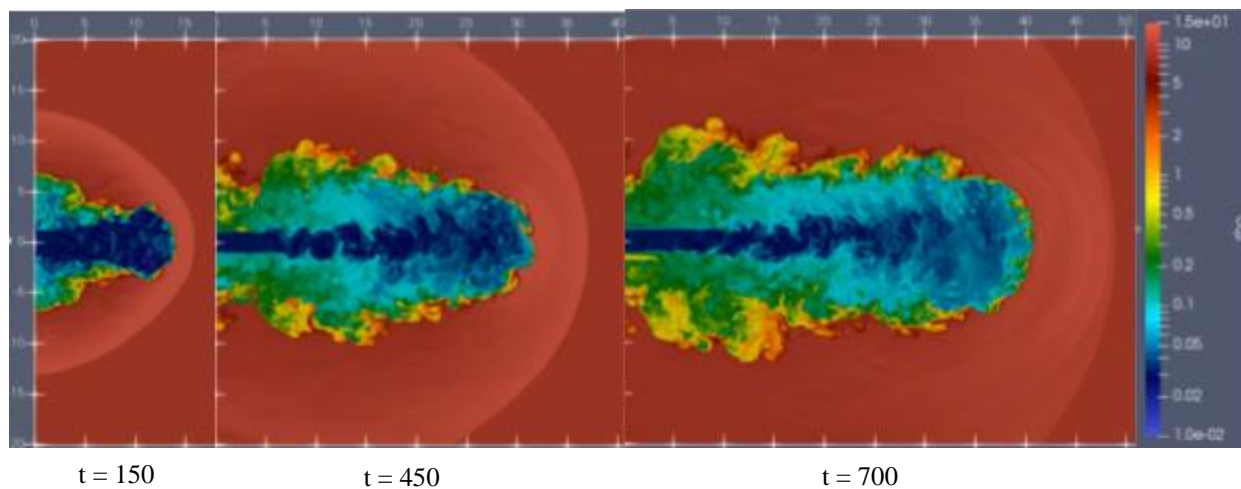


**FIGURE 4.** HHR jet simulation with the same parameters as the HR simulation in Fig. 3,  $v_j = 0.80c$  and  $\eta = 0.00316$ . This simulation is also an FR I type. We see that by  $t = 450$ , the jet has become unstable in the same manner as Fig. 3. As the simulation continues and almost all features propagate further, approaching the edge of the grid, we see that the jet end (dark blue column region) remains nearly fixed at 25 jet radii. Note the progress each jet, Figs. 3 and 4, has made by  $t = 700$ . This is a result of the different resolutions.

take longer, but as a tradeoff we are able to see finer details in the jet. These are the reasons why the jet end does not propagate as far, and it actually means that we have produced an even more realistic simulation.

Albeit this is a brief analysis, the significance in increasing the resolution of our simulations is quite apparent. Also, although the above comparison revealed that both our resolution types resulted in FR I–type jets, we have to realize that that might not always be the case. We could have a HR simulation produce a FR I, but its HHR companion simulation produces a FR II. Knowing this, in the future it would be useful to perform even more HHR simulations of jets that already appear on our HR chart from Fig. 2. This way we can more accurately determine what types of three-dimensional jets are FR I and what types are FR II.

In addition to examining the jet morphologies, as mentioned previously, our work on our highest resolution 3D RHD simulations follows our previous high-resolution 3D RHD jet simulations<sup>15</sup> as well as our 2D RHD jet simulations.<sup>14</sup> Based on what we found, it is worth discussing how the various simulation types compare and why we are justified in assuming the highest resolution three-dimensional modeling is superior. Starting with 2D, we found that the simulations are actually more symmetric than 3D versions because fewer instabilities can be excited in the former. We also found that 2D simulations take longer times to cross the entire grid, and their jet ends are much further behind their corresponding bow shocks than they are in the 3D simulations. The biggest difference we found is that 2D simulations inflate much wider bow shocks and cocoons and therefore we lose information off the grid along the upper and lower boundaries. As expected, we discovered in comparing 2D to 3D that the differences are small, confirming our hypothesis that the 3D approach is not only valid but, indeed, superior.

When we compared the HHR simulations to the HR simulations, we first found that the former required 16 times more computational resources in order to make the two runs identical. This was expected, since we doubled the resolution in all three spatial directions and the time coordinate. We also found that HHR showed far more instabilities, because numerical data that could be seen as negligible in HR was now relevant. This led to more detailed, accurate jets. Consequently, the HR simulation propagated at a higher rate, which was also expected. Overall, our comparisons were mostly expected, and they justified our decision to increase our resolution. That being said, if we were to enhance the resolution even further, we would expect to see even more instabilities materialize. We would also like to think that where the FR I jets become unstable would reach a plateau point, meaning as resolution power increased, the times at which instabilities occur would converge to some absolute value. At that point we would have created simulations that depict, to the best ability, actual observed relativistic jets.

## CONCLUSION

We have simulated an exceptionally large suite of over 50 3D RHD propagating jets using both Athena codes, 12 of which were reproduced at higher resolution. Our simulations of propagating jets have spanned a significant range of velocities (0.7c–0.995c) that cover the great majority of the velocities deduced for radio galaxies.<sup>16</sup> These flows are light, as is appropriate to radio jets, with jet density to ambient medium density ratios ( $\eta$ ) between  $5.0 \times 10^{-4}$  and  $3.2 \times 10^{-2}$ . Both high-resolution (10 zones per jet radius) and higher-resolution (20 zones per radius) simulations have been completed, extending out to 60 jet radii along the direction of motion; in all cases our simulations had widths of 50 jet radii in the two perpendicular directions, so there was no loss of matter out of the grid along those transverse boundaries or the need to worry about waves reflecting off those boundaries and unphysically distorting the jet flow.

These simulations span a sufficient range in power so that the weaker ones are unstable before they pass through our simulation volumes. When scaled to the appropriate extragalactic dimensions and parameters, these cases yield FR I–type morphologies. The majority of our simulations took advantage of the relativistic velocities computable with the two codes and correspond to powerful sources that remain stable for very extended distances and times. On large scales these would be FR II radio galaxies, and on small scales they would be young radio galaxies. Comparisons between our HHR and HR simulations were also made which show that the HR simulations have fewer instabilities and detail, and they take less time to propagate across the entire grid.

In the future we would like to improve our jet simulations even further. This would include continuing to enhance the resolution capabilities of our simulations but also incorporating new factors into our models that we previously neglected for simplicity. An example of this would be using a more complex background medium where the density is nonuniform. This would most likely affect jet stability, but it would create an environment that is even more comparable to what is observed. Lastly, we would like to make more progress with Athena++ by producing fully 3D relativistic magnetohydrodynamic simulations. From there we would then like to produce light curves and power spectral density plots of simulations. This was previously done with the HR simulations to further verify our simulations with observational data. We hope to be able to reproduce those results with our current models. With all these additions, our jets would be even more accurate.

## ACKNOWLEDGMENTS

We acknowledge use of the ELSA High Performance Computing Cluster at The College of New Jersey for conducting the research reported in this paper. ParaView software was used extensively for the production of most of the figures. We also acknowledge our other group members for their great contributions to this work: Geena Elghossain, Nick Juliano, Nick Tusay, and Xuanyi Zhao.

## REFERENCES

1. Y. C. Jiang et al., *Astron. Astrophys.* **469**(1), 331–337 (2007).
2. C. M. Urry and P. Padovani, *Publ. Astron. Soc. Pac.* **107**(715), 803 (1995).
3. B. L. Fanaroff and J. M. Riley, *Mon. Not. R. Astron. Soc.* **167**(1), 31P–36P (1974).
4. Gp. Gopal-Krishna et al., *Mon. Not. R. Astron. Soc.* **314**(4), 815–825 (2000).
5. D. R. Rayburn, *Mon. Not. R. Astron. Soc.* **179**(4), 603–617 (1977).
6. P. J. Wiita, *Astrophys. J.* **221**, 436–448 (1978).
7. M. L. Norman et al., *Astron. Astrophys.* **113**, 285–302 (1982).
8. P. A. G. Scheuer, *Mon. Not. R. Astron. Soc.* **166**(3), 513–528 (1974).
9. R. D. Blandford and M. J. Rees, *Mon. Not. R. Astron. Soc.* **169**(3), 395–415 (1974).
10. T. A. Gardiner and J. M. Stone, *J. Comput. Phys.* **205**(2), 509–539 (2005).
11. J. M. Stone et al., *Astrophys. J. Suppl. Series* **178**(1), 137 (2008).
12. K. Beckwith and J. M. Stone, *Astrophys. J. Suppl. Series* **193**(1), 6 (2011).
13. C. J. White, J. M. Stone, and C. F. Gammie, *Astrophys. J. Suppl. Series* **225**(2), 22 (2016).
14. M. Pollack, D. Pauls, and P. J. Wiita, *Astrophys. J.* **820**(1), 12 (2016).
15. Y. Li et al., *Astrophys. J.* **869**(1), 32 (2018).
16. M. L. Lister et al., *Astronom. J.* **137**(3), 3718 (2009).